Electrical Power and Energy Systems 104 (2019) 524–536

Contents lists available at ScienceDirect

Electrical Power and Energy Systems

journal homepage: www.elsevier.com/locate/ijepes

A distributed optimal reactive power flow for global transmission and distribution network

Jinquan Zhao[a,*], Zhenwei Zhang[a], Jianguo Yao[b], Shengchun Yang[b], Ke Wang[b]

[a] College of Energy and Electrical Engineering, Hohai University, Nanjing 210098, China
[b] State Grid Electric Power Research Institute, Nanjing 210003, China

ARTICLE INFO

Keywords:
Global transmission and distribution network
Optimal reactive power flow
Distributed computation
Heterogeneous decomposition algorithm

ABSTRACT

With the large-scale integration of distributed generators (DGs), the relationships between transmission network (TN) and distribution networks (DNs) are becoming more closely, especially in the aspects of reactive power and voltage. Optimal reactive power flow (ORPF) problems for TN and DNs are not suitable to be solved independently. Due to the fact that TN and DNs are operated by different control centers, a heterogeneous decomposition (HGD) based distributed ORPF method for global transmission and distribution (T&D) networks is presented in this paper. Considering the characteristics of the master–slave structure, the global T&D-ORPF problem can be decomposed into the TN-ORPF master sub-problem, the DN-ORPF slave sub-problems and the boundary consistency coordination sub-problem. Any of those optimization algorithms based on duality and gradient theory can be adopted to solve the TN-ORPF or DN-ORPF sub-problems. By incorporating a penalty function into optimization algorithm, the discrete control variables can successively discretized and therefore the augmented Lagrangian functions are differentiable. Boundary sensitivities constructed by the boundary dual multipliers are used to decouple the global ORPF problem of T&D networks. The same solution as the centralized optimization is achieved by transferring the boundary variables and sensitivities between the TN control center and DN control centers. The simulation results of IEEE 30-bus (TN) and modified IEEE 33-bus (DN) test systems containing multiple DGs show that the HGD algorithm is effective.

1. Introduction

1.1. Background

As a large-scale of distributed generators (DGs) were integrated into distribution networks (DNs) [1], DNs are not suitable to be treated as equivalent loads in transmission network (TN) optimal power flow (OPF) computation. It has brought some new challenges such as voltage rises, congestion issues and balancing [2]. The operating characteristics and control methods of DN have become increasingly complex [3,4].

Generally, the optimal reactive power flow (ORPF) problems of the TN and DNs are solved separately. If the TN can make good use of the reactive power regulation of the controllable devices such as DGs in DNs, it is possible to maximize the overall interests at a smaller cost. Reactive voltage relations between the TN and DNs are much tighter than ever before. Therefore, the voltage regulation capability of the TN should be sufficiently utilized to help DNs eliminate their overvoltage problems, as well as to reduce network losses. Integrated solutions to the T&D ORPF problem, to this effect, have remarkable research significance.

The TN and DNs are operated and controlled by different control centers of power grids, thus the T&D-ORPF is a distributed optimization problem of interconnected networks. A decomposition technique should be adopted for the integrated power networks to achieve global objective. The decomposition algorithm adopted for interconnected power networks must function independently of the control center and not overly burden the communication system.

1.2. Previous researches

Existing decomposed optimization algorithms can be roughly split into three categories: Lagrange relaxation [5–9], Karush-Kuhn-Tucker (KKT) decomposition [10,11] and Benders decomposition [12]. Lagrange relaxation techniques include the classic Lagrangian relaxation (CLR) [7] and the augmented Lagrangian relaxation (ALR) [5,6,8,9]. CLR is achieved by adding the consistency constraint of the boundary variables into the Lagrangian function of the OPF problem, then decomposing the Lagrangian function according to the saddle point

* Corresponding author.
E-mail address: jqzhao2@tom.com (J. Zhao).

https://doi.org/10.1016/j.ijepes.2018.07.019
Received 7 February 2018; Received in revised form 19 June 2018; Accepted 11 July 2018
Available online 25 July 2018

theorem. Thus, the optimization problem is decomposed into a series of regional sub-optimization problems and the update of the boundary multipliers based on optimal gradient. As an extension to CLR, the ALR contains an additional boundary constraint quadratic term, and features enhanced convergence. However, the separation of Lagrangian function is destroyed due to the quadratic term, many methods are investigated for decomposing this quadratic term, including the auxiliary problem principle (APP) [5] and the alternating direction method of multipliers (ADMM) [8,9]. In KKT decomposition methods, the extended Hessian matrix of global KKT optimality conditions is decomposed directly into some sub extended Hessian matrixes for sub-area power networks [10,11]. Benders decomposition is a distributed method for specific models which are comprised of a master optimal sub-problem and multiple independent slave optimal sub-problems. Feasible cuts are formed in slave sub-problems to correspond with the master problem [12].

The T&D networks have a unique master-slave structure. Generally, the TN regards a DN as an equivalent load and the DN regards the TN as an infinite equivalent generator. The global ORPF problem of T&D networks is decoupled by the gateway power (or voltage) limits provided by the automatic voltage controller (AVC) [13,14]. Theoretical support for this kind of methods is yet relatively weak, and the extensive bilateral interactions between neighbor networks have yet to be thoroughly investigated.

There have been a deal of researches on simulation and operation problems of global T&D networks in recent years. A distributed power flow for T&D networks was proposed in [15,16], named master-slave-splitting (MSS) method, the voltage magnitude and the exchange power at boundary buses are used as coordination variables. In [17], a novel MSS iterative method was developed for solving the global T&D state estimation (SE) problem. In the MSS method, with introducing the boundary fictitious measurements, the global SE problem was split into a TN SE sub-problem and a number of DN SE sub-problems. In [18], a distributed continuation power flow based on master-slave structure was presented to assess voltage stability of integrated T&D networks. The generalized Benders decomposition (GBD) was applied to decompose the global T&D ORPF problem [12]. In GBD, the slave sub-problems are the ORPF problem of DNs, and the master sub-problem is the ORPF problem of the TN. The global T&D OPF problem was decomposed heterogeneously and the feasible cuts constraints are used to transfer the impacts caused by the adjacent networks. The generation of feasible cuts is very difficult for GBD, and the quality and efficiency of problem solving are affected heavily by them. A coordinated economic dispatch method of integrated T&D networks based on heterogeneous decomposition (HGD) was proposed in [19] and an integrated T&D contingency analysis was proposed in [20]. Later on, a HGD based distributed active OPF method of global T&D networks is presented [21]. In HGD, the global T&D OPF problem was decomposed heterogeneously and the boundary sensitivities are used to transfer the impacts caused by the adjacent networks. The optimal solution can be obtained by exchanging the boundary variables and the sensitivities. Compared to APP, ADMM, or KKT decomposition methods, the HGD method has better independence and adaptability for decomposing T&D OPF problems with a master-slave structure. Numerical simulations show that a decomposition algorithm can speed up the convergence if it can follow the master-slave structure of TN and DN [21].

1.3. Contributions

A distributed ORPF for integrated T&D networks based on HGD is proposed in this paper. The global ORPF problem is decomposed into the TN-ORPF master sub-problem, DN-ORPFs slave sub-problems and the boundary consistency coordination sub-problem. Any of the existing optimization algorithms based on duality theory can be adopted to solve the TN-ORPF or DN-ORPF sub-problems. Moreover, the presence of a large number of discrete control variables makes it more difficult to solve. By incorporating a penalty function into the ORPF algorithm, the discrete control variables can be successively discretized and therefore the augmented Lagrangian functions are differentiable. Comparison of the proposed approach with ADMM method has been provided in Appendix A, as well as the relevant analysis.

It is necessary to note that since the reverse power flow may occur in both low-voltage DN [22,24] and medium-voltage DN [23,25] with high penetration of DGs, both the forward boundary active and reactive power flows and reverse power flows are accepted within its acceptable range in this paper. Related agreements between TN and DNs on bi-directional active-reactive power flows should be signed under the TN operation security requirements.

The contributions of this paper are summarized as follows:

1) HGD method proposed in [21] is developed to handle the global T&D ORPF problem. It was decomposed into a TN-ORPF master sub-problem, some DN-ORPF slave sub-problems and the boundary consistency coordination sub-problem. The independence of TN and DN computation in different control centers are satisfied.
2) A penalty function approach for handling the discrete variables is used to solve the distributed T&D ORPF problem and the augmented Lagrangian functions are differentiable. It is shown that the HGD algorithm can be extended to solve the mixed-integer nonlinear programming problems.

This paper is organized as follows. Section 2 describes the integrated reactive power optimization model and decomposition of the global T&D networks. Then, Section 3 gives the detailed distributed ORPF model of T&D networks. Next, algorithm and implementation of distributed computation between TN control center and DN control centers are demonstrated in Section 4. Numerical simulations with IEEE 30 and 33-bus system are performed to show that the HGD algorithm is effective in Section 5. Finally, the main conclusions are presented in Section 6.

2. Formulation and decomposition of global T&D ORPF problem

2.1. The global T&D ORPF problem formulation

In this work, the generator reactive power, on-load tap changers (OLTC) and capacitor banks (CB) are investigated in TN-ORPF problem. The static var compensator (SVC), DGs with various control characteristics and CBs will be considered in DN-ORPF problem.

Fig. 1 shows the global T&D networks. The TN and k^{th} DN are connected at the k^{th} PCC (point of common couple) bus $(k = 1, 2, \cdots, N_{\text{Dis}})$.

The global T&D ORPF problem can be formulated as follows:

$$\min.\quad f_{\text{T}}(\mathbf{u}_{\text{T}}, \mathbf{x}_{\text{T}}, \Omega_{\mathbf{x}_{\text{pcc},k}}) + \sum_{k=1}^{N_{\text{Dis}}} f_{\text{D}_k}(\mathbf{u}_{\text{D}_k}, \mathbf{x}_{\text{D}_k}, \mathbf{x}_{\text{pcc},k}) \tag{1}$$

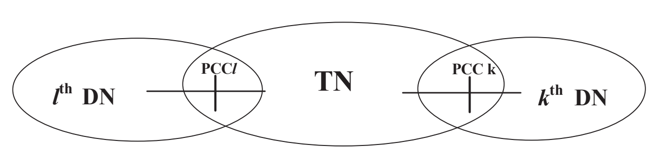

Fig. 1. Diagram of integrated transmission and distribution network.

$$s.\,t.\quad \mathbf{h}_{\mathrm{T}}(\mathbf{u}_{\mathrm{T}}, \mathbf{x}_{\mathrm{T}}, \mathbf{x}_{\mathrm{pcc},k}) = 0 \tag{2}$$

$$\mathbf{g}_{\mathrm{T}}(\mathbf{u}_{\mathrm{T}}, \mathbf{x}_{\mathrm{T}}) \leqslant 0 \tag{3}$$

$$\mathbf{h}_{\mathrm{D}_k}(\mathbf{u}_{\mathrm{D}_k}, \mathbf{x}_{\mathrm{D}_k}, \mathbf{x}_{\mathrm{pcc},k}) = 0 \quad k = 1, \cdots, N_{\mathrm{Dis}} \tag{4}$$

$$\mathbf{g}_{\mathrm{D}_k}(\mathbf{u}_{\mathrm{D}_k}, \mathbf{x}_{\mathrm{D}_k}) \leqslant 0 \quad k = 1, \cdots, N_{\mathrm{Dis}} \tag{5}$$

$$\mathbf{h}_{pcc.k}(\mathbf{x}_{\mathrm{T}}, \mathbf{x}_{\mathrm{pcc},k}, \mathbf{x}_{\mathrm{D}_k}) = 0 \quad k = 1, \cdots, N_{\mathrm{Dis}} \tag{6}$$

$$\mathbf{g}_{pcc,k}(\mathbf{x}_{\mathrm{pcc},k}) \leqslant 0 \quad k = 1, \cdots, N_{\mathrm{Dis}} \tag{7}$$

where the TN and k^{th} DN are denoted by T and D_k respectively; $\mathbf{x}_{\mathrm{T}}$, $\mathbf{x}_{\mathrm{D}_k}$ and $\mathbf{x}_{\mathrm{pcc},k}$ are the state variable vector of the TN, the k^{th} DN and their common couple buses (PCC k) respectively; $\Omega_{\mathbf{x}_{\mathrm{pcc},k}}$ is the collections of $\mathbf{x}_{\mathrm{pcc},k}$; $\mathbf{u}_{\mathrm{T}}$ and $\mathbf{u}_{\mathrm{D}_k}$ are the controllable variable vector of the TN and the k^{th} DN respectively; is the number of DNs; f_{T} and f_{D_k} are objective functions of the TN and k^{th} DN respectively; $\mathbf{h}_{\mathrm{T}}$ and $\mathbf{h}_{\mathrm{D}_k}$ are the power flow equations of the TN and k^{th} DN (except the PCC bus) respectively; $\mathbf{g}_{\mathrm{T}}$ and $\mathbf{g}_{\mathrm{D}_k}$ are the inequality constraints of the TN and k^{th} DN (except the PCC bus) respectively; $\mathbf{h}_{pcc,k}$ and $\mathbf{g}_{pcc,k}$ are the boundary power flow equations and inequality constraints of PCC k respectively.

2.2. Global T&D ORPF problem splitting

A new variable vector is introduced, named $\mathbf{S}_{\mathrm{pcc},k}$, which represents the transmitted power from the TN to the k^{th} DN. The decomposed boundary equality constraints (6) can be written as follow:

$$\begin{cases} \mathbf{h}_{\mathrm{T},pcc,k}(\mathbf{x}_{\mathrm{T}}, \mathbf{x}_{\mathrm{pcc},k}) = \mathbf{S}_{\mathrm{pcc}k} \\ \mathbf{S}_{\mathrm{pcc}k} = \mathbf{h}_{\mathrm{D}_k,pcc}(\mathbf{x}_{\mathrm{pcc}k}, \mathbf{x}_{\mathrm{D}_k}) \end{cases} \quad k = 1, \cdots, N_{\mathrm{Dis}} \tag{8}$$

where $\mathbf{h}_{\mathrm{T},pcc,k}$ and $\mathbf{h}_{\mathrm{D}_k,pcc}$ are the boundary equality constraints of the TN and the k^{th} DN after decomposition.

The proposed distributed HGD algorithm for solving ORPF in this paper was developed to extend the original HGD method for solving decomposed OPF problem proposed in [21]. Based on the HGD algorithm, the distributed model derivation of global T&D ORPF problem is described in detail in Appendix B.

The global T&D ORPF problem can be decomposed into a TN-ORPF master sub-problem and DN-ORPF slave sub-problems and the boundary consistency coordination sub-problem. Then the communications and coordination between the TN control center and DN control centers are shown in Fig. 2.

The mathematical model of the TN-ORPF master sub-problem can be written as:

$$\min \quad \mathrm{f}_{\mathrm{T}}^{*} = \mathrm{f}_{\mathrm{T}} + \sum_{\mathrm{k}=1}^{\mathrm{N_{Dis}}} \alpha_{\mathrm{k}}^{\mathrm{T}} \mathbf{X}_{\mathrm{pcc,k}} \tag{9}$$

$$s.\,t.\quad \mathbf{h}_{\mathrm{T}}(\mathbf{u}_{\mathrm{T}}, \mathbf{x}_{\mathrm{T}}) = 0 \tag{10}$$

$$\mathbf{g}_{\mathrm{T}}(\mathbf{u}_{\mathrm{T}}, \mathbf{x}_{\mathrm{T}}) \leqslant 0 \tag{11}$$

$$\mathbf{h}_{T,pcc,k}(\mathbf{x}_{\mathrm{T}}, \mathbf{x}_{\mathrm{pcc}k}) = \widetilde{\mathbf{S}}_{\mathrm{pcc}k} \quad k = 1, \cdots, N_{\mathrm{Dis}} \tag{12}$$

$$\mathbf{g}_{pcc,k}(\mathbf{x}_{\mathrm{pcc}k}) \leqslant 0 \quad k = 1, \cdots, N_{\mathrm{Dis}} \tag{13}$$

The mathematical model of k^{th} DN-ORPF slave sub-problem can be written as:

$$\min \quad f_{\mathrm{D}_k}^{*} = f_{\mathrm{D}_k} + \widetilde{\beta}_k^{\mathrm{T}} \mathbf{S}_{pcc,k} \tag{14}$$

$$s.\,t.\quad \mathbf{h}_{\mathrm{D}_k}(\mathbf{u}_{\mathrm{D}_k}, \mathbf{x}_{\mathrm{D}_k}) = 0 \tag{15}$$

$$\mathbf{g}_{\mathrm{D}_k}(\mathbf{u}_{\mathrm{D}_k}, \mathbf{x}_{\mathrm{D}_k}) \leqslant 0 \tag{16}$$

$$\mathbf{S}_{\mathrm{pcc}k} = \mathbf{h}_{\mathrm{D}_k,pcc}(\widetilde{\mathbf{x}}_{\mathrm{pcc}k}, \mathbf{x}_{\mathrm{D}_k}) \tag{17}$$

where the superscript '$\sim$' indicates that the variable is fixed in this sub-problem.

According to the TN-ORPF sub-problem in (9)(13), the boundary bus is taken as a load bus in TN control center, $\widetilde{\mathbf{S}}_{\mathrm{pcc}k}$ is regard as a fixed value. And in the slave sub-problem (14)(17), the boundary bus is taken as the slave bus in k^{th} DN control center, $\widetilde{\mathbf{x}}_{\mathrm{pcc}k}$ is also regard as a fixed value.

Based this decomposition method, the traditional management ways of TN and DN control centers are retained. The same solution as the centralized optimization is realized by alternately solving the TN-ORPF and DN-ORPF sub-problems and exchanging their boundary variable vectors and sensitivities. If the boundary sensitivities and variables are all close enough to results of the last iteration, it is considered that it satisfies the consistency criteria.

3. Distributed computation of global T&D networks ORPF

3.1. The TN-ORPF formulation

The TN-ORPF sub-problem contains continuous and discrete variables (e.g., OLTCs and CBs). The TN-ORPF master sub-problem can be formulated in detail as:

$$\min \quad f_{\mathrm{T}}^{*} = \sum_{i,j\in\Omega_{\mathrm{T}}} -G_{ij}\left(\frac{1}{K_{ij}}V_i^2 + K_{ij}V_j^2 - 2V_iV_j\cos\theta_{ij}\right) + \sum_{k=1}^{N_{\mathrm{Dis}}} \widetilde{\alpha}_k^{\mathrm{T}} \mathbf{x}_{\mathrm{pcc},k} \tag{18}$$

$$s.\,t.\quad P_{G,i} - P_{d,i} - V_i \sum_{j\in\Omega_{\mathrm{T}}} V_j(G_{ij}\cos\theta_{ij} + B_{ij}\sin\theta_{ij}) = 0 \quad i \in \Omega_{\mathrm{T}} \tag{19}$$

$$Q_{G,i} - Q_{d,i} + V_i^2 C_i - V_i \sum_{j\in\Omega_{\mathrm{T}}} V_j(G_{ij}\sin\theta_{ij} - B_{ij}\cos\theta_{ij}) = 0 \quad i \in \Omega_{\mathrm{T}} \tag{20}$$

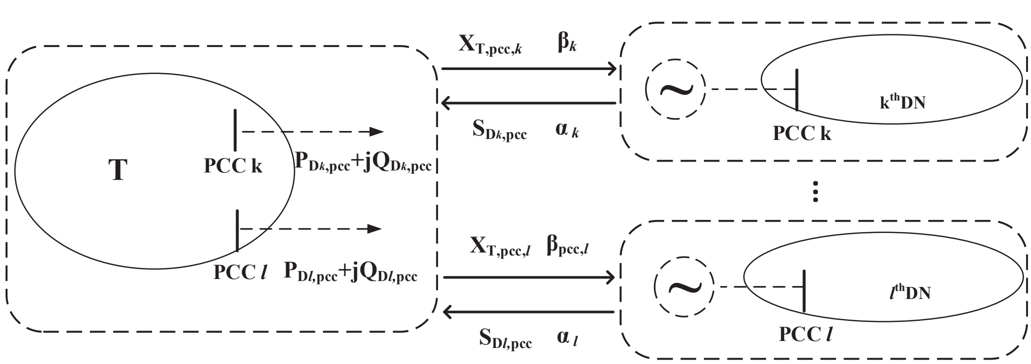

Fig. 2. Decomposition and communication of the ORPF for transmission and distribution network.

$$Q_{G,i,\min} \leqslant Q_{G,i} \leqslant Q_{G,i,\max} \quad i \in \Omega_{T,G} \tag{21}$$

$$K_{ij,\min} \leqslant K_{ij} \leqslant K_{ij,\max} \quad i \in \Omega_{T,K} \tag{22}$$

$$V_{i,\min} \leqslant V_i \leqslant V_{i,\max} \quad i \in \Omega_T \tag{23}$$

$$C_{i,\min} \leqslant C_i \leqslant C_{i,\max} \quad i \in \Omega_{T,C} \tag{24}$$

where $\mathbf{x}_{pcck} = [V_{T,pcc,k} \;\; \theta_{T,pcc,k}]^T$; Ω_T, $\Omega_{T,G}$, $\Omega_{T,K}$ and $\Omega_{T,C}$ are collections of buses, generator buses, transformer branches and capacitor buses in TN, respectively; V_i and θ_i are the i^{th} bus voltage magnitude and angle; $\theta_{ij} = \theta_i - \theta_j$; G_{ij} and B_{ij} are the conductance and susceptance between i^{th} bus and j^{th} bus; $P_{d,i}$ and $Q_{d,i}$ are the load active and reactive power at i^{th} bus, respectively; $P_{G,i}$ and $Q_{G,i}$ are the active and reactive output of generators at i^{th} bus, respectively; $Q_{G,i,\max}$ and $Q_{G,i,\min}$ are the upper and lower limits of $Q_{G,i}$, respectively; K_{ij} is the ratio of OLTC at the branch between i^{th} bus and j^{th} bus; $K_{ij,\max}$and $K_{ij,\min}$ are the upper and lower limits ofK_{ij}, respectively; C_i is the susceptance of CB at i^{th} bus; $C_{i,\max}$ and $C_{i,\min}$ are the upper and lower limits of C_i, respectively; $V_{i,\max}$ and $V_{i,\min}$ are the upper and lower limits of V_i, respectively; α_k^T can be computed by the k^{th} DN, as follows:

$$\alpha_k = \begin{bmatrix} \frac{\partial f_{D_k}}{\partial V_{D_k,pcc}} \\ \frac{\partial f_{D_k}}{\partial \theta_{D_k,pcc}} \end{bmatrix} - \begin{bmatrix} \frac{\partial \mathbf{h}_{D_k}}{\partial V_{D_k,pcc}} \\ \frac{\partial \mathbf{h}_{D_k}}{\partial \theta_{D_k,pcc}} \end{bmatrix} \mathbf{y}_{D_k} - \begin{bmatrix} \frac{\partial \mathbf{g}_{D_k}}{\partial V_{D_k,pcc}} \\ \frac{\partial \mathbf{g}_{D_k}}{\partial \theta_{D_k,pcc}} \end{bmatrix} \omega_{D_k} + \begin{bmatrix} \frac{\partial \mathbf{h}_{D_k,pcc}}{\partial V_{D_k,pcc}} \\ \frac{\partial \mathbf{h}_{D_k,pcc}}{\partial \theta_{D_k,pcc}} \end{bmatrix} \mathbf{y}_{D_k,pcc} \tag{25}$$

where $V_{D_k,pcc}$ and $\theta_{D_k,pcc}$ are the bus voltage magnitudes and angles of bus PCC k in the k^{th} DN; $V_{T,pcc,k}$ and $\theta_{T,pcc,k}$ are the bus voltage magnitudes and angles of bus PCC k in the TN, respectively.

3.2. The k^{th} DN-ORPF sub-problem formulation

The model of k^{th} DN considers continuous (e.g. the SVC, DGs with various control characteristics) and discrete variables (CBs). The k^{th} DN-ORPF problem can be formulated as:

$$\min \quad f_{D_k}^* = \sum_{i,j \in \Omega_{D_k}} -G_{ij}(V_i^2 + V_j^2 - 2V_iV_j\cos\theta_{ij}) + \widetilde{\beta}_k^T \mathbf{S}_{pcck} \tag{26}$$

$$s.\,t. \quad P_{DG,i} - P_{d,i} - V_i \sum_{j \in \Omega_{D_k}} V_j(G_{ij}\cos\theta_{ij} + B_{ij}\sin\theta_{ij}) = 0 \qquad i \in \Omega_{D_k} \tag{27}$$

$$Q_{DR,i} - Q_{d,i} + V_i^2 C_i - V_i \sum_{j \in \Omega_{D_k}} V_j(G_{ij}\sin\theta_{ij} - B_{ij}\cos\theta_{ij}) = 0 \quad i \in \Omega_{D_k} \tag{28}$$

$$Q_{DR,i,\min} \leqslant Q_{DR,i} \leqslant Q_{DR,i,\max} \quad i \in \Omega_{DR} \tag{29}$$

$$I_{DGI,i,\min} \leqslant I_{DGI,i} \leqslant I_{DGI,i,\max} \quad i \in \Omega_{DGI} \tag{30}$$

$$V_{i,\min} \leqslant V_i \leqslant V_{i,\max} \quad i \in \Omega_{D_k} \tag{31}$$

$$C_{i,\min} \leqslant C_i \leqslant C_{i,\max} i \in \quad \Omega_C \tag{32}$$

$$P_{D_k,pcc,\min} \leqslant P_{D_k,pcc} \leqslant P_{D_k,pcc,\max} \tag{33}$$

$$Q_{D_k,pcc,\min} \leqslant Q_{D_k,pcc} \leqslant Q_{D_k,pcc,\max} \tag{34}$$

where Ω_{D_k}, Ω_{DR} and Ω_C are collections of buses, reactive power supply (DG or SVC) buses and capacitor buses in k^{th} DN, respectively; Ω_{DGI} is bus collections of current controlled DG, $\Omega_{DGI} \subset \Omega_{DR}$; $P_{DG,i}$ is the active power output of DG at i^{th} bus; $Q_{DR,i}$ is the reactive output of reactive power supply at i^{th} bus; $Q_{DR,i,\max}$ and $Q_{DR,i,\min}$ are the upper and lower limits of $Q_{DR,i}$; $I_{DGI,i}$ are the DG current magnitudes at i^{th} bus; $I_{DGI,i,\max}$ and $I_{DGI,i,\min}$ are the upper and lower limits of $I_{DGI,i}$; $\beta_k = \mathbf{y}_{T,pcc,k}$, can be computed by TN; $\mathbf{S}_{pcck} = [P_{D_k,pcc} \;\; Q_{D_k,pcc}]^T$, $P_{D_k,pcc}$ and $Q_{D_k,pcc}$ are the active and reactive power of bus PCC k in the k^{th} DN; $P_{D_k,pcc,\min}$ and $P_{D_k,pcc,\min}$ are the upper and lower limits of $P_{D_k,pcc}$; $Q_{D_k,pcc,\max}$ and $Q_{D_k,pcc,\min}$ are the upper and lower limits of $Q_{D_k,pcc}$. (33) and (34) are the boundary power constraints.

3.3. Reactive capability limits of DG

Reactive power capacity of current and voltage controlled DG interface inverters are discussed in this section. The reactive capability limits of such a DG can be determined in relation to the maximum current, maximum voltage and maximum active power output.

1. The reactive power capability of voltage controlled DG is always affected by its interface inverter capacity [26].

$$Q_{DG,max} = \sqrt{S_{\max}^2 - P_{DG}^2} \tag{35}$$

$$Q_{DG,min} = -Q_{DG,max} \tag{36}$$

where $Q_{DG,max}$ and $Q_{DG,min}$ are the upper and lower reactive power output limits of the DG; $S_{\max}$ is the upper apparent power capacity limit of inverter; P_{DG} is the active power output of the DG.

The reactive capability limits of the current controlled DGs are affected by current limits, voltage magnitudes, and active output [27], can be expressed as:

$$Q_{DG,\max} = \sqrt{V_{DG}^2 I_{DG,\max}^2 - P_{DG}^2} \tag{37}$$

$$Q_{DG,\min} = 0 \tag{38}$$

where V_{DG} is the voltage magnitudes of DG; $I_{DG,\max}$ is the upper limit of current magnitude of DG.

3.4. Communication mechanism and convergence criteria

Boundary variable vectors and sensitivities are transferred between TN control center and DN control centers, and iterate asynchronously until the boundary consistency criteria are satisfied. In the k^{th} iteration process, if the boundary variables and sensitivities of TN and DNs are all close enough to results of the last iteration, it is considered that it satisfies the consistency criteria. The consistency criteria are expressed as:

$$\max_{k=1,\cdots,N_{Dis}} \{|P_{D_k,pcc}^m - P_{D_k,pcc}^{m-1}|\} \leqslant \varepsilon \tag{39}$$

$$\max_{k=1,\cdots,N_{Dis}} \{|Q_{D_k,pcc}^m - Q_{D_k,pcc}^{m-1}|\} \leqslant \varepsilon \tag{40}$$

$$\max_{k=1,\cdots,N_{Dis}} \{|V_{D_k,pcc}^{m+1} - V_{D_k,pcc}^m|\} \leqslant \varepsilon \tag{41}$$

$$\max_{k=1,\cdots,N_{Dis}} \{|\theta_{D_k,pcc}^{m+1} - \theta_{D_k,pcc}^m|\} \leqslant \varepsilon \tag{42}$$

$$\max_{k=1,\cdots,N_{Dis}} \{\|\alpha_k^m - \alpha_k^{m-1}\|\} \leqslant \varepsilon \tag{43}$$

$$\max_{k=1,\cdots,N_{Dis}} \{\|\beta_k^{m+1} - \beta_k^{m-1}\|\} \leqslant \varepsilon \tag{44}$$

where ε is the given tolerance; the superscript m marks the m^{th} distributed iterative calculation between TN and DNs control centers; $|*|$ is the absolute value of $*$; $\|*\|$ is the 2-Norm of vector $*$.

4. Algorithm and implementation of distributed computation

4.1. Algorithm for solving ORPF sub-problem

Any of those optimization algorithms based on duality and gradient theory (e.g. primal-dual interior point method [29], Newton's method

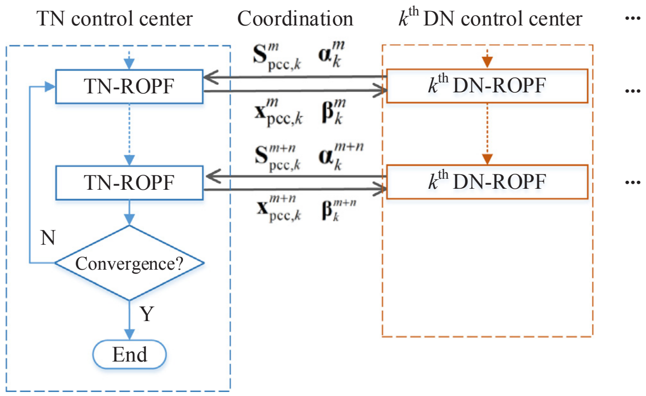

Fig. 3. Flowchart of the distributed ORPF based on HGD algorithm.

[28]) can be adopted to solve the ORPF sub-problems. The penalty function methods (e.g. Gaussian penalty function [29] and polynomial penalty function [28] or sinusoidal penalty function [30]) can be used to relax the discrete variables to continuous and therefore the augmented Lagrangian functions are differentiable. In this paper's simulation, the primal-dual interior point algorithm incorporated the Gaussian penalty function (described in detail in [29]) is adopted to solve both TN-ORPF and DN-ORPF sub-problems.

4.2. Implementation of distributed computation

The procedure of the proposed distributed computation is shown as below:

Step 1: Set the iteration counter $m = 1$, the initial value of boundary bus voltage magnitude and angle in each DN are 1 and 0 (p.u.), respectively, and set the initial boundary sensitivity as [0;0];

Step 2: Each DN-ORPF sub-problem is solved in its DN control center respectively, then the $P^m_{Dk,pcc} + jQ^m_{Dk,pcc}$ and α^m_k are obtained and sent to TN control center;

Step 3: The TN-ORPF sub-problem is solved in the TN control center, then the $V^m_{T,pcc,k}$, $\theta^m_{T,pcc,k}$ and β^m_k are obtained and sent to each DN control center;

Step 4: If the convergence criteria are satisfied, terminate the iteration; else set $m = m + 1$ and go to Step 2.

The coordinative relations and iterative process between of TN control center and each DN control centers are shown in Fig. 3.

4.3. Discussion of convergence

The proposed distributed HGD algorithm for solving ORPF in this paper was actually developed to extend the original HGD method for solving decomposed OPF problem in [21]. The convergence of this method was proved to have a local one-order convergence rate under some conditions and be equivalent to a fixed point iterative problem, which can be seen in [21]. The addition of the penalty functions for handling the discrete variables does not change the whole proof since the corresponding partial differential terms does not affect the boundary sensitivities.

Like all of those large-scale nonlinear programming problems, when some contradictory inequality constraints are given in some engineering application cases, the distributed computation would be divergent and the ORPF problem would be unsolvable. When they are happened, some heuristic schemes, such as identifying bad inequality constraint based on the abnormal (too big) dual multipliers and relaxing them, to be used to obtain the sub-optimal solution. In engineering application, if they are happened, the distributed computation process can be terminated and turn back to the independent ORPF computation mode when these heuristic schemes do not work.

Table 1
Buses and parameters of DGs in IEEE33.

DG Types	Control strategies	Bus	Parameters/p.u.
Gas turbine	PQ decoupled	4,8	P = 0.03, V = 1, Smax = 0.05
Photovoltaic generation	Current	15	P = 0.03, Imax = 0.05

Table 2
Buses and parameters of DGs in IEEE69.

DG Types	Control strategies	Bus	Parameters/p.u.
Gas turbine	PQ decoupled	11,33	P = 0.03, V = 1, Smax = 0.08
Photovoltaic generation	Current	44,63,67	P = 0.03, Imax = 0.06

5. Numerical simulations

5.1. Introduction to the text system and data

An integrated test system is constructed by an IEEE 30-bus or IEEE 118-bus as TN system, and several IEEE33-bus or IEEE69-bus as DN systems. The DN system is connected to the load bus (PCC) of TN. The power standard value of TN system is 100 MW, and that of the DN system is 10 MW. The base voltage of the IEEE30 or IEEE118 system is 135 kV, and that of the IEEE33 or IEEE69 system is 12.66 kV. The voltage limit is set to ± 5% of the nominal voltage.

In the IEEE 30-bus or 118-bus system, the values of CBs are all limits to 0–0.3p.u., and step size is 0.05p.u.. The tap value of OLTC is limit to 0.95–1.05p.u. and the step size is 0.01p.u.

In the modified IEEE33-bus system, four DGs are connected to buses 4, 8 and 15 (DG4, DG8, DG15) respectively. A SVC is connected to buses 29 (SVC 29#). The reactive power capacity of SVC is [−0.3, 0.3] Mvar. Two CBs are connected to buses 10 (CB 10#) and 24 (CB 24#) respectively. Their values all are [0, 0.03] p.u. and the step size is 0.005. The limits of boundary active/reactive power in modified IEEE33-bus system is [−4, 4] MW and [−3, 3] Mvar. Referred to reactive capability limits of DG, part parameters and control strategies related to DGs are given in Table 1.

In the modified IEEE69-bus system, five DGs are connected to buses 11#, 33#, 44#, 53#, and 67#, respectively. A SVC is connected to buses 23 (SVC 23#). The reactive power capacity of SVC is [−0.7, 0.7] Mvar. Two CBs are connected to buses 18 (CB 18#) and 50 (CB 50#) respectively. Their values are all [0, 0.03] p.u. and step sizes are 0.005.

Table 3
Bus voltage magnitudes comparison of different algorithms on T-D system.

Value	Network losses/MW			Voltage magnitude of PCC/p.u.		
Algorithm	Sep	Cen	Dis	PF	Cen	Dis
D26	0.0809	0.0779	0.0779	1.0066	1.0281	1.0281
T	5.1019	5.0720	5.0721	–	–	–
Total	5.1828	5.1499	5.1500	–	–	–

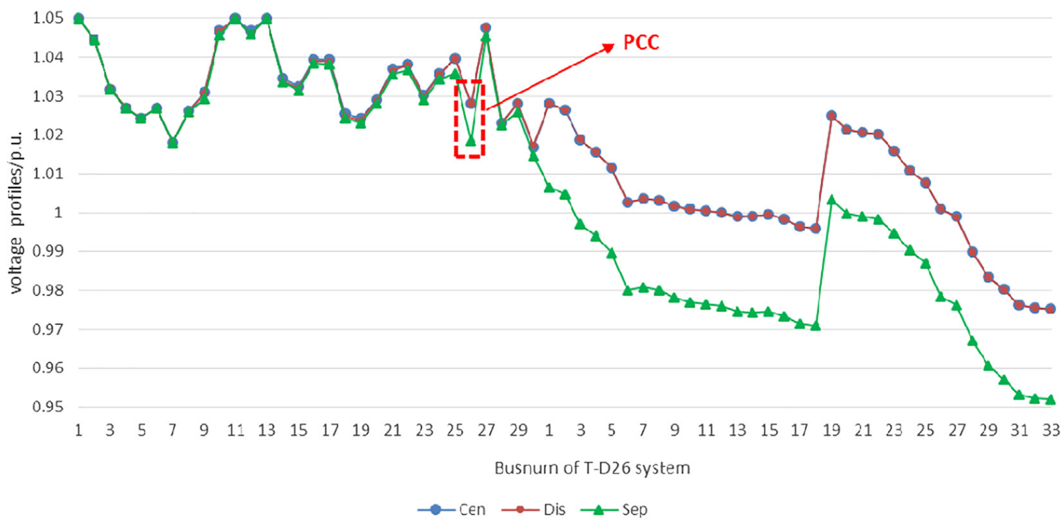

Fig. 4. Voltage profiles with different algorithms on T-D system.

The limits of boundary active/reactive power in modified IEEE69-bus system is [−6, 6] MW and [−4, 4] Mvar. Referred to reactive capability limits of DG, part parameters and control strategies related to DGs are given in Table 2.

5.2. Case A: T-D

An IEEE33-bus systems connects to the IEEE30-bus systems at bus 26 (named PCC26) of the IEEE30-bus systems. This case named T-D. The proposed HGD distributed method (hereafter named Dis) is compared to a centralized optimization method (hereafter named Cen) and a separated optimization method (hereafter named Sep). Centralized optimization method means the ORPF problems of TN and DNs is solved in one control center. Separated optimization method means the ORPF problems of TN and DNs are solved in their own control centers without coordination. Set $\varepsilon = 10^{-5}$ in the criterion (9).

The comparisons of results are shown in Table 3.

The iteration process of HGD method converges within 6 times. From Table 3, it can be found that, the HGD method is effective since its results are very close to the centralized optimization. Comparisons of voltage amplitudes of all buses are shown in Fig. 4. Comparison of control results with different algorithms is shown in Fig. 5.

Table 4
Results comparison of different algorithms on T-3D system.

Value	Network losses/MW		Voltage magnitude of PCC/p.u.	
Algorithm	Sep	Dis	PF	Dis
D7	0.0815	0.0778	1.0032	1.0191
D19	0.0793	0.0792	1.0159	1.0288
D26	0.0836	0.0775	0.9982	1.0305
T	5.1019	5.0346	–	–
Total	5.3563	5.2691	–	–

As is shown in Fig. 4, the voltage magnitudes of HGD method are similar to centralized optimization. Thus the voltage of PCC bus is supported and higher than that with separated optimization. Fig. 5 shows that the control results of centralized optimization method are similar to the HGD method.

5.3. Case B: T-3D

Three IEEE33-bus systems connect to the IEEE30-bus system at bus

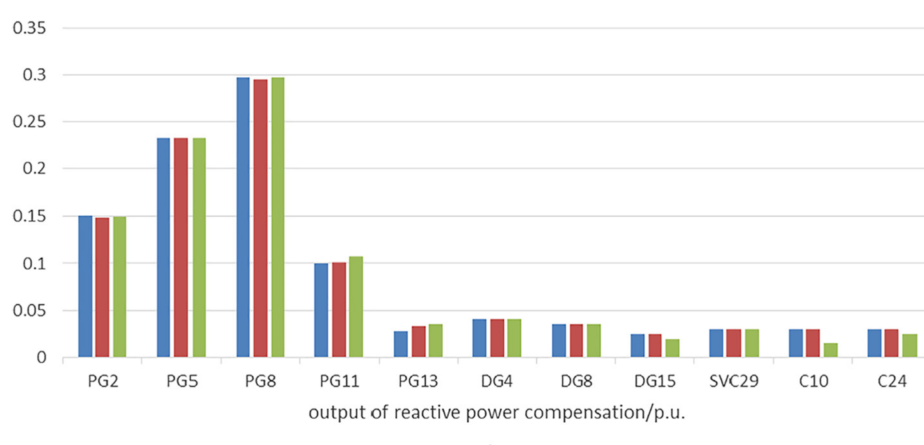

Fig. 5. Output comparison of control results with different algorithms on T-D system.

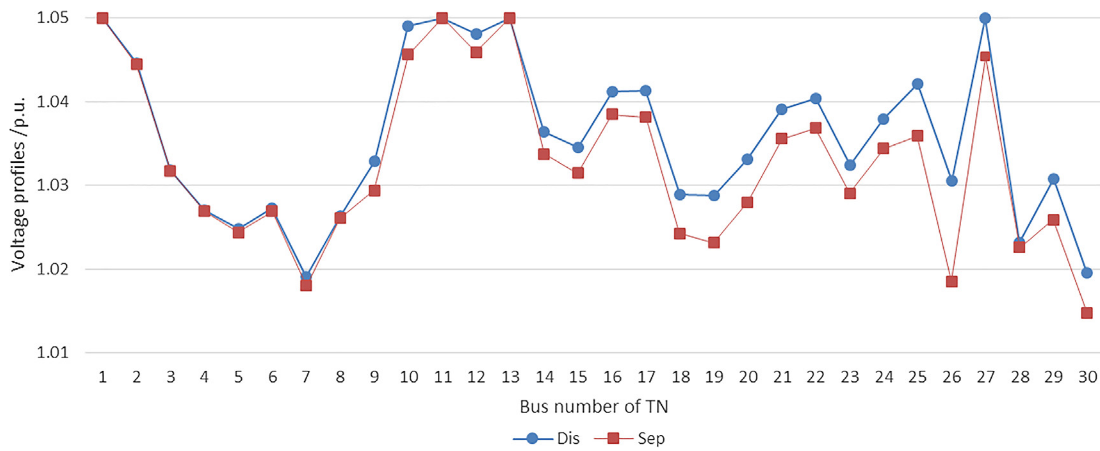

Fig. 6. Voltage profiles of TN with different algorithms on T-3D system.

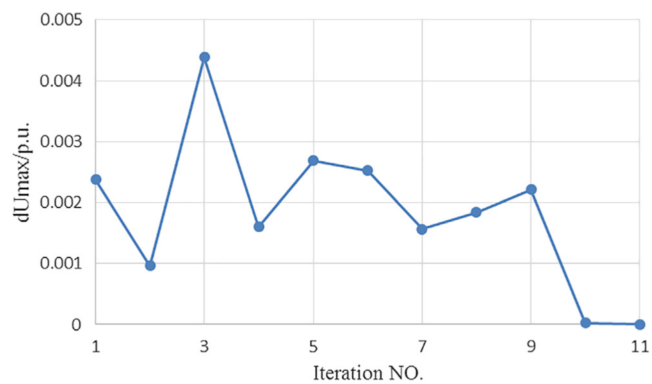

Fig. 7. Change of maximum voltage criterion deviation of all PCC bus with iteration.

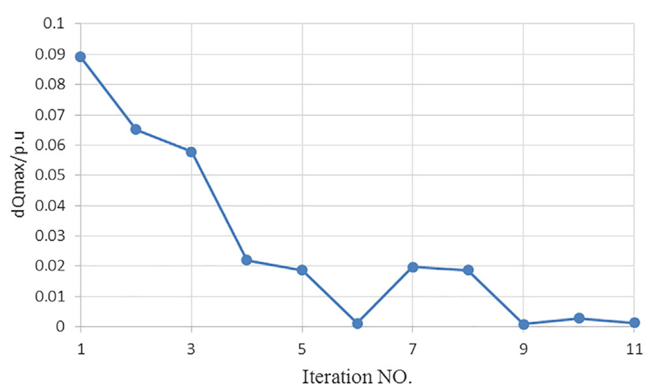

Fig. 8. Change of maximum reactive power criterion deviation of all PCC bus with iteration.

7, 19 and 26 (named PCC7, PCC19, PCC26) of IEEE30-bus system respectively. This case named T-3D. In this case, the IEEE33-bus systems named D7, D19 and D26 respectively. The results are shown in Table 4 and Fig. 6. The change of maximum voltage criterion deviation of all PCC bus with iteration are shown Fig. 7. The change of maximum reactive power criterion deviation of all PCC bus with iteration are shown Fig. 8. The change of each boundary active/reactive power with iteration are shown Figs. 9, 10.

The results show that the HGD algorithm can be used to solve the distributed reactive power optimization of the transmission network and the distribution networks. The mutual influence between the transmission network and distribution network can be fully reflected by exchanging light boundary information.

Set $\mathrm{d}U_{\max} = \max\limits_{k=7,19,26}\{|V^{m+1}_{\mathrm{D}_k,pcc} - V^{m}_{\mathrm{D}_k,pcc}|\}$, is the maximum voltage criterion deviation of all PCC bus, and its change with iteration is shown in Fig. 8. Set $\mathrm{d}Q_{\max} = \max\limits_{k=7,19,26}\{|Q^{m}_{\mathrm{D}_k,pcc} - Q^{m-1}_{\mathrm{D}_k,pcc}|\}$, is the maximum reactive power criterion deviation of all PCC bus, and its change with iteration is shown in Fig. 9.

Figs. 7, 8 show that the voltage and reactive power criterion deviation both tend towards a decrease characteristic with iteration until convergence. It shows that good convergence on this case study.

Figs. 9, 10 show the change of boundary active/reactive power with iteration. It shows that each boundary active power or reactive power changes with iteration and tends to be stable until convergence.

5.4. Case C: T-5D

Two IEEE33-bus systems connect to the IEEE118-bus system at bus 7 and 26 (named PCC7, PCC26) respectively. And three IEEE69-bus systems connect to the IEEE118-bus system at bus 16, 19 and 28 (named PCC16, PCC37, PCC48) respectively. This case named T-5D. The results are shown in Table 5.

The results show that when mixed integer HGD algorithm is used to solve large-scale transmission and distribution network system, it also has good convergence and practicality.

5.5. Time comparison

The HGD method converges with 6, 11 and 12 times on T-D, T-3D and T-5D system respectively. The time comparisons of different methods to solve these systems are shown in Table 6.

It can be seen from the Table 6, the computing time on T-D case with centralized optimization method is shorter than HGD method. But the computing time on T-5D case with centralized optimization method is similar to the HGD method. In HGD method, the distribution network can be calculated in parallel in the iteration process. In the centralized optimization, the difficulty and time of calculation are significantly increased with the more of the distribution networks added in the case. However, the difficulty or time of calculation do not increase obviously

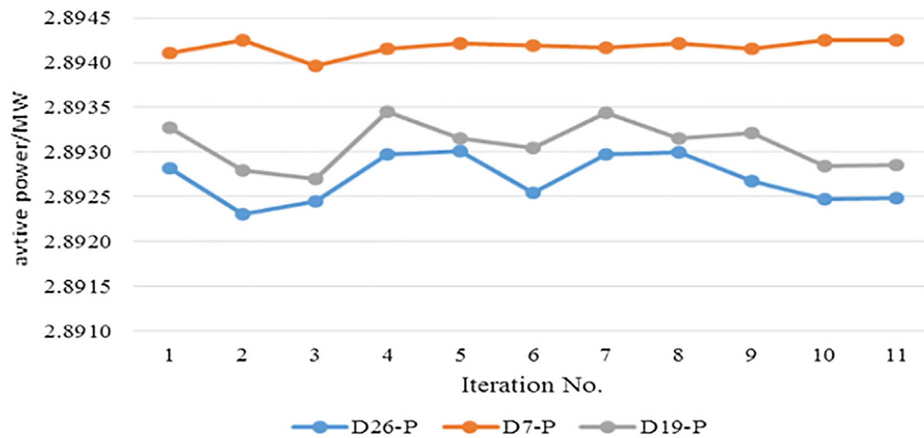

Fig. 9. Change of each boundary active power with iteration.

with more distribution networks. Therefore, the more distribution networks in the actual project, the advantages of the distributed algorithm will become more and more prominent.

6. Conclusion

In this paper, a distributed method for global T&D ORPF problem is presented. The global ORPF problem can be decomposed into a TN-ORPF master sub-problem, several DN-ORPF slave sub-problems and the boundary consistency coordination sub-problem. Coordination between the TN control center and DN control centers is achieved by transferring boundary variables and sensitivities. In this paper's simulation, the primal-dual interior point algorithm incorporated the Gaussian penalty function is adopted to solve both TN-ORPF and DN-ORPF sub-problems, then the discrete control variables can successively discretized and therefore the augmented Lagrangian functions are differentiable. Simulations under different computation modes show that the HGD method yields the same results as centralized calculation.

The focus of this study was static optimal reactive power flow. A hybrid algorithm combined with the current HGD and other time decoupling methods can be used to solve multi-time TD-ORPF problem, which may be investigated in future studies.

Table 5
Results comparison of different algorithms on T-5D system.

Value	Network losses/MW		Voltage magnitude of PCC/p.u.	
Algorithm	Sep	Dis	PF	Dis
D7	0.0815	0.0792	1.0032	1.0195
D26	0.0836	0.0775	0.9982	1.0309
D16	0.0729	0.0724	1.0221	1.0239
D37	0.0697	0.0694	1.0406	1.0431
D48	0.0736	0.0714	1.0159	1.0297
T	111.0513	106.0601	–	–
Total	111.4326	106.4300	–	–

Table 6
Time comparison of different algorithms on three case of T-D system.

Time/s	Sep.	Cen.	HGD.
T-D	3.3	1.890	8.319
T-3D	3.5	7.269	19.430
T-5D	5.4	47.3	55.2

Acknowledgements

This work is a part of the National Key R&D Program of China (NO. 2017YFB0902600) and the General Program of National Natural Science Foundation of China (NO. 51577049). The authors would like to thank for the supports from the National Key R&D Program of China and the National Natural Science Foundation of China.

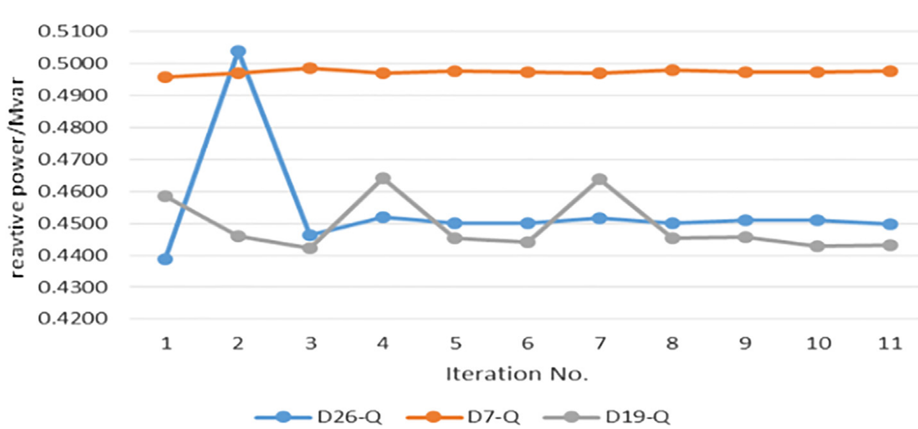

Fig. 10. Change of each boundary reactive power with iteration.

Appendix A

Analysis of the difference of the HGD and ADMM

1, Global T&D ORPF problem splitting based on ADMM algorithm

The general model of global ORPF problem for transmission and distribution network can be expressed as

$$\min.\quad f_{\mathrm{T}}(\mathbf{u}_{\mathrm{T}}, \mathbf{x}_{\mathrm{T}}, \Omega\mathbf{x}_{\mathrm{T},pcc,k}, \Omega\mathbf{s}_{\mathrm{T},pcc,k}) + \sum_{k\in\Omega_{dis*}} f_{\mathrm{D}_k}(\mathbf{u}_{\mathrm{D}_k}, \mathbf{x}_{\mathrm{D}_k}, \mathbf{x}_{\mathrm{D}_k,\mathrm{pcc}}, \mathbf{s}_{\mathrm{D}_k,\mathrm{pcc}}) \tag{A-1}$$

$$s.\ t.\quad \mathbf{h}_{\mathrm{T}}(\mathbf{u}_{\mathrm{T}}, \mathbf{x}_{\mathrm{T}}, \Omega\mathbf{x}_{\mathrm{T},pcc,k}, \Omega\mathbf{s}_{\mathrm{T},pcc,k}) = 0 \tag{A-2}$$

$$\mathbf{g}_{\mathrm{T}}(\mathbf{u}_{\mathrm{T}}, \mathbf{x}_{\mathrm{T}}, \Omega\mathbf{x}_{\mathrm{T},pcc,k}, \Omega\mathbf{s}_{\mathrm{T},pcc,k}) \leqslant 0 \tag{A-3}$$

$$\mathbf{h}_{\mathrm{D}_k}(\mathbf{u}_{\mathrm{D}_k}, \mathbf{x}_{\mathrm{D}_k}, \mathbf{x}_{\mathrm{D}_k,\mathrm{pcc}}, \mathbf{s}_{\mathrm{D}_k,\mathrm{pcc}}) = 0 \quad k\in\Omega_{dis*} \tag{A-4}$$

$$\mathbf{g}_{\mathrm{D}_k}(\mathbf{u}_{\mathrm{D}_k}, \mathbf{x}_{\mathrm{D}_k}, \mathbf{x}_{\mathrm{D}_k,\mathrm{pcc}}, \mathbf{s}_{\mathrm{D}_k,\mathrm{pcc}}) \leqslant 0 \quad k\in\Omega_{dis*} \tag{A-5}$$

$$\mathbf{x}_{D_k,\mathrm{pcc}} = \mathbf{x}_{T,pcc,k} \quad k\in\Omega_{dis*} \tag{A-6}$$

$$\mathbf{S}_{\mathrm{D}_k,\mathrm{pcc}} = \mathbf{S}_{\mathrm{T},pcc,k} \quad k\in\Omega_{dis*} \tag{A-7}$$

where, Ω_{dis*} is a collections of distribution networks connected to the transmission network. The objective function in (A-1) is to minimize the operation objective of TN and DNs; the Eqs. (A-2) and (A-4) are the power flow equations of the TN and k^{th} DN respectively; the Eqs. (A-3) and (A-5) are the inequality constraints of the TN and k^{th} DN respectively; the Eqs. (A-6) and (A-7) are are the constraints of boundary variable vectors.

Based on the ADMM method, the augmented Lagrange function is as follows:

$$L_G = f_{\mathrm{T}} - \mathbf{y}_{\mathrm{T}}^{\mathrm{T}}\mathbf{h}_{\mathrm{T}} - \mathbf{w}_{\mathrm{T}}^{\mathrm{T}}\mathbf{g}_{\mathrm{T}} + \sum_{k\in\Omega_{dis*}}\Big(f_{\mathrm{D}_k} - \mathbf{y}_{\mathrm{D}_k}^{\mathrm{T}}\mathbf{h}_{\mathrm{D}_k} - \mathbf{w}_{\mathrm{D}_k}^{\mathrm{T}}\mathbf{g}_{\mathrm{D}_k} - \lambda_{k,s}(\mathbf{S}_{\mathrm{T},pcc,k} - \mathbf{S}_{\mathrm{D}_k,pcc}) - \lambda_{k,x}(\mathbf{x}_{\mathrm{T},pcc,k} - \mathbf{x}_{\mathrm{D}_k,pcc}) + \frac{\rho_{k,s}}{2}\|\mathbf{S}_{\mathrm{T},pcc,k} - \mathbf{S}_{\mathrm{D}_k,pcc}\| + \frac{\rho_{k,x}}{2}\|\mathbf{x}_{\mathrm{T},pcc,k} - \mathbf{x}_{\mathrm{D}_k,pcc}\|\Big) \tag{A-8}$$

where, $\lambda_{k,s}$, $\lambda_{k,x}$ are the lagrange multiplier of constraints (A-6) and (A-7): $\rho_{k,x}$, $\rho_{k,s}$ are the penalty parameters, $\rho_{k,x}\in R^{+}$, $\rho_{k,s}\in R^{+}$.Based on ADMM method, the iterative format of distributed optimization problem of transmission and distribution grid is as follows:

$$\left(\mathbf{u}_{\mathrm{T}}^{m+1}, \mathbf{x}_{\mathrm{T}}^{m+1}, \Omega\mathbf{x}_{\mathrm{T},pcc,k}^{m+1}, \Omega\mathbf{s}_{\mathrm{T},pcc,k}^{m+1}\right) = \operatorname{argmin}.L_G\left(\mathbf{u}_{\mathrm{T}}, \mathbf{x}_{\mathrm{T}}, \Omega\mathbf{x}_{\mathrm{T},pcc,k}, \Omega\mathbf{s}_{\mathrm{T},pcc,k}, \mathbf{u}_{\mathrm{D}_k}^{m}, \mathbf{x}_{\mathrm{D}_k}^{m}, \Omega\mathbf{x}_{\mathrm{D}_k,pcc}^{m}, \Omega\mathbf{s}_{\mathrm{D}_k,pcc}^{m}, \Omega\lambda_{k,s}^{m}, \Omega\lambda_{k,x}^{m}\right) \tag{A-9}$$

$$(\mathbf{u}_{\mathrm{D}_k}^{m+1}, \mathbf{x}_{\mathrm{D}_k}^{m+1}, \mathbf{x}_{\mathrm{D}_k,pcc}^{m+1}, \mathbf{s}_{\mathrm{D}_k,pcc}^{m+1}) = \operatorname{argmin}.L_G(\mathbf{u}_{\mathrm{T}}^{m+1}, \mathbf{x}_{\mathrm{T}}^{m+1}, \mathbf{x}_{\mathrm{T},pcc,k}^{m+1}, \mathbf{s}_{\mathrm{T},pcc,k}^{m+1}, \mathbf{u}_{\mathrm{D}_k}, \mathbf{x}_{\mathrm{D}_k}, \mathbf{x}_{\mathrm{D}_k,pcc}, \mathbf{s}_{\mathrm{D}_k,pcc}, \lambda_{k,s}^{m}, \lambda_{k,x}^{m})k\in\Omega_{dis*} \tag{A-10}$$

The Lagrangian multipliers are updated iteratively as follows by simply applying the sub-gradient method until the interconnecting variables on both interconnected regions match:

$$\lambda_{k,s}^{m+1} = \lambda_{k,s}^{m} + \rho_s^{m+1}(\mathbf{S}_{\mathrm{T},pcc,k}^{m+1} - \mathbf{S}_{\mathrm{D}_k,pcc}^{m+1})k\in\Omega_{dis*} \tag{A-11}$$

$$\lambda_{k,x}^{m+1} = \lambda_{k,x}^{m} + \rho_x^{m+1}(\mathbf{x}_{\mathrm{T},pcc,k}^{m+1} - \mathbf{x}_{\mathrm{D}_k,pcc}^{m+1})k\in\Omega_{dis*} \tag{A-12}$$

The stopping criterion for solving the decomposed regional ORPF problem is that the maximum mismatch between coupling variables is smaller than a preset threshold value:

$$\max_{k\in\Omega_{dis*}}\left\{\left\|\begin{bmatrix}\mathbf{r}^m\\ \mathbf{d}^m\end{bmatrix}\right\|\right\} \leqslant \varepsilon \tag{A-13}$$

where, $\mathbf{r}_k^m = [\mathbf{S}_{\mathrm{T},pcc,k}^m - \mathbf{S}_{\mathrm{D}_k,pcc}^m;\mathbf{x}_{\mathrm{T},pcc,k}^m - \mathbf{x}_{\mathrm{D}_k,pcc}^m]$; $\mathbf{d}_k^m = [\mathbf{S}_{\mathrm{T},pcc,k}^m - \mathbf{S}_{\mathrm{T},pcc,k}^{m-1};\mathbf{x}_{\mathrm{D}_k,pcc}^m - \mathbf{x}_{\mathrm{D}_k,pcc}^{m-1}]$,$\varepsilon = 10^{-5}$.

2, Numerical simulations

In the modified IEEE33-bus system, two more DGs are connected to buses 25 and 32 respectively. The distribution network takes bus 15# as a local slack bus. Referred to reactive capability limits of DG, part parameters and control strategies related to DGs are given in Table A-1.

The primal-dual interior point algorithm incorporated the Gaussian penalty function is adopted to solve both TN-ORPF and DN-ORPF sub-problems. The results are shown in Table A-2.

Compared with the separated optimization, the results of ADMM distributed optimization are better. The results show that the coordination between the control centers can be realized by ADMM distributed computing. However, the HGD algorithm shows better coordination. Moreover, the convergence of ADMM algorithm is related to the selection of those penalty parameters. When ADMM is applied in this case, where $\rho_{k,x}$ = [0.1;0.1] $\rho_{k,s}$ = [0.1;0.1], it can converge in 50 iterations.

Table A-1

DG Types	Control strategies	Bus	Parameters/p.u.
DG1	PQ decoupled	4,8	P = 0.03, V = 1, $S_{\max}$ = 0.05
DG3	Slack bus	15	V = 1.05, $P_{\max}$ = 0.07; $P_{\max}$ = −0.07; $Q_{\max}$ = 0.07; $Q_{\min}$ = −0.07
DG4	Current	23	P = 0.03, $I_{\max}$ = 0.05
DG5	PQ decoupled	25,32	P = 0.02, $Q_{\max}$ = 0.03; $Q_{\min}$ = −0.03

Table A-2

Algorithm	Network losses MW			Voltage magnitude of PCC/p.u.		
	Sep.	ADMM	HGD	Sep.	ADMM	HGD
D26	0.1925	0.0251	0.0249	0.9583	0.9722	0.9967
T	5.1015	5.0542	5.0134	1.0147	0.9722	0.9967
Total	5.2940	5.0793	5.0383	–	–	–

And it can converge in 30 iterations with the HGD. Simulations also show that the decomposition algorithm can speed up the convergence if it can follow the master-slave structure of TN and DN.

3. Analysis of the difference of the HGD and ADMM algorithm

The advantages of the HGD method are as follows:

1) The HGD algorithm is inspired by the heterogeneous operational characteristics of transmission network and distribution network. The T&D networks have a unique master-slave structure, the decoupling of HGD can be more consistent with the decoupling characteristics of the transmission and distribution network. Generally, the interconnected regional transmission networks are decomposed into a series of homogeneous sub-systems with nearly identical data characteristics at the boundary buses, as illustrated in the following figure. However, the T&D networks have a unique master-slave structure, the TN control center regards a DN system as an equivalent load bus and the DN control center regards the TN system as the root bus. Based on the HGD decomposition principle, the ORPF problem of T&D network can be decomposed into sub-problems with heterogeneous data structures of the boundary buses. Moreover, there is a significant difference between the scale of transmission network and distribution network, which is not conducive to convergence. Simulations show that the decomposition algorithm can speed up the convergence if it can follow the master-slave structure of TN and DN [21].
2) The HGD algorithm does not use the external coordination layer to update the multiplier and the loosened coupling constraint as the penalty factor for the decomposition of the target.
3) The convergence rate of the ADMM algorithm is closely related to the selection of the Lagrange multiplier and the penalty parameter. The HGD needn't introduce the multipliers and the penalty factor to relax the coupling constraints into the objective for decomposition, and the penalty regulation issue is thus avoided because of the different decomposition principles.

Appendix B

The proposed distributed HGD algorithm for solving ORPF in this paper was developed to extend the original HGD method for solving decomposed OPF problem proposed in [21]. Based on the HGD algorithm, the decomposition process of the global T&D ORPF problem is as follow:

The Lagrangian function of global T&D ORPF problem can be formulated as follow:

$$L_G = f_{\rm T} - \mathbf{y}_{\rm T}^{\rm T}\mathbf{h}_{\rm T} - \mathbf{w}_{\rm T}^{\rm T}\mathbf{g}_{\rm T} - \sum_{k=1}^{N_{\rm Dis}} \mathbf{w}_{{\rm pcc},k}^{\rm T}\mathbf{g}_{{\rm pcc},k} - \sum_{k=1}^{N_{\rm Dis}} \mathbf{y}_{{\rm T},pcc,k}^{\rm T}(\mathbf{h}_{{\rm T},pcc,k} - \mathbf{S}_{{\rm pcc}k}) + \sum_{k=1}^{N_{\rm Dis}} (f_{{\rm D}_k} - \mathbf{y}_{{\rm D}_k}^{\rm T}\mathbf{h}_{{\rm D}_k} - \mathbf{w}_{{\rm D}_k}^{\rm T}\mathbf{g}_{{\rm D}_k} - \mathbf{y}_{D_k,pcc}^{\rm T}(\mathbf{S}_{{\rm pcc}k} - \mathbf{h}_{{\rm D}k,pcc})) \tag{B-1}$$

where L_G is the Lagrangian function of reactive power optimization for global T&D; $\mathbf{y}_{\rm T}$ $\mathbf{w}_{\rm T}$ are Lagrangian dual multiplier vectors of equality constraints and inequality constraints in TN respectively; $\mathbf{y}_{{\rm D}_k}$ $\mathbf{w}_{{\rm D}_k}$ are Lagrangian dual multiplier vectors of equality constraints and inequality constraints in $k^{\rm th}$ DN respectively; $\mathbf{y}_{{\rm T},pcc,k}$ $\mathbf{w}_{{\rm pcc},k}$ are Lagrangian dual multiplier vectors of equality constraints and inequality constraints of PCCk bus respectively; some new auxiliary functions, named $f_{{\rm T},pcc,k}$, $f_{{\rm D}k,{\rm pcc}}$, are introduced to represent the impact of $k^{\rm th}$ DN and TN on each other respectively. Then the objective function can be decomposed as follow:

$$\min \quad F_{\rm T} = f_{\rm T} + \sum_{k=1}^{N_{\rm Dis}} f_{{\rm T},pcc,k} \tag{B-2}$$

$$\min \quad F_{{\rm D}_k} = f_{{\rm D}_k} + f_{{\rm D}_k,{\rm pcc}} \quad k = 1, \cdots, N_{\rm Dis} \tag{B-3}$$

where $F_{\rm T}$, $F_{{\rm D}_k}$ are decomposed objective functions of TN-ORPF and $k^{\rm th}$ DN-ORPF sub-problem respectively.

The augmented Lagrangian function of reactive power optimization for TN and $k^{\rm th}$ DN ORPF sub-problems are formulated as follow:

$$L_{{\rm G}-T} = F_{\rm T} - \mathbf{y}_{\rm T}^{\rm T}\mathbf{h}_{\rm T} - \mathbf{w}_{\rm T}^{\rm T}\mathbf{g}_{\rm T} - \sum_{k=1}^{N_{\rm Dis}} \mathbf{w}_{{\rm pcc}k}^{\rm T}\mathbf{g}_{{\rm pcc}k} - \sum_{k=1}^{N_{\rm Dis}} \mathbf{y}_{{\rm T},pcc,k}^{\rm T}(\mathbf{h}_{{\rm T},pcc,k} - \widetilde{\mathbf{S}}_{{\rm pcc}k}) \tag{B-4}$$

$$L_{{\rm G}-D_k} = f_{{\rm D}_k} - \mathbf{y}_{{\rm D}_k}^{\rm T}\mathbf{h}_{{\rm D}_k} - \mathbf{w}_{{\rm D}_k}^{\rm T}\mathbf{g}_{{\rm D}_k} - \mathbf{y}_{D_k,pcc}^{\rm T}(\mathbf{S}_{{\rm pcc}k} - \mathbf{h}_{D_k,pcc}) + f_{D_k,pcc} \tag{B-5}$$

where $L_{{\rm G}-T}$ and $L_{{\rm G}-{\rm D}_k}$ are the Lagrangian function of reactive power optimization for TN and $k^{\rm th}$ DN ORPF sub-problems; $\mathbf{y}_{\rm T}$ and $\mathbf{w}_{\rm T}$ are Lagrangian dual multiplier vectors of the equality constraints and the inequality constraints in TN respectively; $\mathbf{y}_{{\rm D}_k}$ and $\mathbf{w}_{{\rm D}_k}$ are Lagrangian dual multiplier vectors of the equality constraints and the inequality constraints in $k^{\rm th}$ DN respectively; $\mathbf{y}_{{\rm T},pcc,k}$ and $\mathbf{w}_{{\rm pcc},k}$ are Lagrangian dual multiplier vectors of the equality constraints and the inequality constraints of PCCk bus respectively; the top 'T' indicates transposition of the vector or matrix; set $L_{\rm T} = f_{\rm T} - \mathbf{y}_{\rm T}^{\rm T}\mathbf{h}_{\rm T} - \mathbf{w}_{\rm T}^{\rm T}\mathbf{g}_{\rm T} - \sum_{k=1}^{N_{\rm Dis}} \mathbf{w}_{{\rm pcc}k}^{\rm T}\mathbf{g}_{{\rm pcc}k}$ and $L_{{\rm D}_k} = f_{{\rm D}_k} - \mathbf{y}_{{\rm D}_k}^{\rm T}\mathbf{h}_{{\rm D}k} - \mathbf{w}_{{\rm D}_k}^{\rm T}\mathbf{g}_{{\rm D}_k}$.

The first-order KKT conditions of global T&D ORPF, and distributed T&D ORPF problem can be simplified to write as (B-6) and (B-7), respectively.

$$\frac{\partial L_G}{\partial(\Phi_{\rm T}, \Phi_{{\rm D}_k}, \Omega_{\Phi_{{\rm pcc},k}})} = 0 \tag{B-6}$$

$$\begin{cases} \dfrac{\partial L_{G-T}}{\partial(\Phi_{\mathrm{T}}, \Omega_{\Phi_{\mathrm{pcc},k}})} = 0 \\ \dfrac{\partial L_{G-D_k}}{\partial(\Phi_{\mathrm{D}_k}, \Phi_{\mathrm{pcc}k})} = 0 k = 1, \cdots, N_{\mathrm{Dis}} \end{cases} \tag{B-7}$$

where, Φ_{T}, Φ_{D_k} and $\Phi_{\mathrm{pcc},k}$ are the variable vector collections (e.g. state variable vector, controllable variable vector and Lagrangian dual multiplier vectors) of TN, DN and PCC k$^{\mathrm{th}}$ bus, respectively; $\Phi_{\mathrm{T}} = \{\mathbf{x}_{\mathrm{T}}, \mathbf{u}_{\mathrm{T}}, \mathbf{y}_{\mathrm{T}}, \mathbf{w}_{\mathrm{T}}\}$; $\Phi_{\mathrm{D}_k} = \{\mathbf{x}_{\mathrm{D}_k}, \mathbf{u}_{\mathrm{D}_k}, \mathbf{y}_{\mathrm{D}_k}, \mathbf{w}_{\mathrm{D}_k}\}$; $\Phi_{\mathrm{pcc},k} = \{\mathbf{S}_{\mathrm{pcc}k}, \mathbf{x}_{\mathrm{pcc},k}\mathbf{y}_{\mathrm{T},pcc,k}, \mathbf{w}_{\mathrm{pcc}k}, \mathbf{y}_{D_k,pcc}\}$; $\Omega_{\Phi_{\mathrm{pcc},k}}$ is the collections of $\Phi_{\mathrm{pcc},k}$.

In order to get the same results as the centralized optimization, the formula (B-6) is equivalent to the formula (B-7).

The formula (B-6) can be described in detail as follows:

$$\frac{\partial L_G}{\partial(\Phi_{\mathrm{T}}, \Phi_{\mathrm{D}_k}, \Omega_{\Phi_{\mathrm{pcc},k}})} = 0 \Leftrightarrow \begin{cases} \dfrac{\partial L_G}{\partial \mathbf{x}_{\mathrm{T}}} = \dfrac{\partial L_{\mathrm{T}}}{\partial \mathbf{x}_{\mathrm{T}}} - \sum_{k=1}^{N_{\mathrm{Dis}}} \dfrac{\partial \mathbf{h}_{\mathrm{T},pcc,k}}{\partial \mathbf{x}_{\mathrm{T}}} \mathbf{y}_{T,pcc,k} = 0 \quad \dfrac{\partial L_G}{\partial \mathbf{y}_{\mathrm{T}}} = -\mathbf{h}_{\mathrm{T}} = 0 \dfrac{\partial L_G}{\partial \mathbf{w}_{\mathrm{T}}} = -\mathbf{g}_{\mathrm{T}} = 0 k \\ \dfrac{\partial L_G}{\partial \mathbf{u}_{\mathrm{T}}} = \dfrac{\partial L_{\mathrm{T}}}{\partial \mathbf{u}_{\mathrm{T}}} = 0 \end{cases}$$

$$= 1, \cdots, N_{\mathrm{Dis}} \begin{cases} \dfrac{\partial L_G}{\partial \mathbf{x}_{\mathrm{D}_k}} = \dfrac{\partial L_{\mathrm{D}_k}}{\partial \mathbf{x}_{\mathrm{D}_k}} + \dfrac{\partial \mathbf{h}_{\mathrm{D}_k,\mathrm{pcc}}}{\partial \mathbf{x}_{\mathrm{D}_k}} \mathbf{y}_{D_k,pcc} = 0 \\ \dfrac{\partial L_G}{\partial \mathbf{u}_{\mathrm{D}_k}} = \dfrac{\partial L_{\mathrm{D}_k}}{\partial \mathbf{u}_{\mathrm{D}_k}} = 0 \\ \dfrac{\partial L_G}{\partial \mathbf{y}_{\mathrm{D}_k}} = -\mathbf{h}_{\mathrm{D}_k} = 0 \\ \dfrac{\partial L_G}{\partial \mathbf{w}_{\mathrm{D}_k}} = -\mathbf{g}_{\mathrm{D}_k} = 0 \\ \dfrac{\partial L_G}{\partial \mathbf{x}_{\mathrm{pcc},k}} = \dfrac{\partial L_{\mathrm{T}}}{\partial \mathbf{x}_{\mathrm{pcc},k}} - \dfrac{\partial \mathbf{h}_{\mathrm{T},pcc.k}}{\partial \mathbf{x}_{\mathrm{pcc}.k}} \mathbf{y}_{\mathrm{T}.pcc.k} + \dfrac{\partial L_{\mathrm{D}_k}}{\partial \mathbf{x}_{\mathrm{pcc}.k}} + \dfrac{\partial \mathbf{h}_{\mathrm{D}_k\mathrm{pcc}}}{\partial \mathbf{x}_{\mathrm{pcc}.k}} \mathbf{y}_{\mathrm{D}_k,pcc} = 0 \\ \dfrac{\partial L_G}{\partial \mathbf{S}_{\mathrm{pcc}k}} = \mathbf{y}_{\mathrm{T},pcc,k} - \mathbf{y}_{\mathrm{D}_k,pcc} = 0 \\ \dfrac{\partial L_G}{\partial \mathbf{y}_{\mathrm{T},pcc,k}} = -\mathbf{h}_{\mathrm{T},pcc,k} + \mathbf{S}_{\mathrm{pcc}k} = 0 \\ \dfrac{\partial L_G}{\partial \mathbf{w}_{\mathrm{pcc}k}} = -\mathbf{g}_{\mathrm{pcc}k} = 0 \\ \dfrac{\partial L_G}{\partial \mathbf{y}_{D_k,pcc}} = -\mathbf{S}_{\mathrm{pcc}k} + \mathbf{h}_{\mathrm{D}_k\mathrm{pcc}} = 0 \end{cases} \tag{B-8}$$

And the formula (B-7) can be described in detail as follows:

$$\frac{\partial L_{G-T}}{\partial(\Phi_{\mathrm{T}}, \Omega_{\Phi_{\mathrm{pcc},k}})} = 0 \Leftrightarrow \begin{cases} \dfrac{\partial L_{G-T}}{\partial \mathbf{x}_{\mathrm{T}}} = \dfrac{\partial L_{\mathrm{T}}}{\partial \mathbf{x}_{\mathrm{T}}} - \sum_{k=1}^{N_{\mathrm{Dis}}} \left(\dfrac{\partial \mathbf{h}_{T,pcc,k}}{\partial \mathbf{x}_{\mathrm{T}}} \mathbf{y}_{\mathrm{T},pcc,k} + \dfrac{\partial f_{\mathrm{T},pcc,k}}{\partial \mathbf{x}_{\mathrm{T}}}\right) = 0 \\ \dfrac{\partial L_{G-T}}{\partial \mathbf{u}_{\mathrm{T}}} = \dfrac{\partial L_{\mathrm{T}}}{\partial \mathbf{u}_{\mathrm{T}}} - \sum_{k=1}^{N_{\mathrm{Dis}}} \dfrac{\partial f_{\mathrm{T},pcc,k}}{\partial \mathbf{u}_{\mathrm{T}}} = 0 \\ \dfrac{\partial L_{G-T}}{\partial \mathbf{y}_{\mathrm{T}}} = -\mathbf{h}_{\mathrm{T}} + \dfrac{\partial f_{\mathrm{T},pcc,k}}{\partial \mathbf{y}_{\mathrm{T}}} = 0 \\ \dfrac{\partial L_{G-T}}{\partial \mathbf{w}_{\mathrm{T}}} = -\mathbf{g}_{\mathrm{T}} + \dfrac{\partial f_{\mathrm{T},pcc,k}}{\partial \mathbf{w}_{\mathrm{T}}} = 0 \\ \dfrac{\partial L_{G-T}}{\partial \mathbf{x}_{\mathrm{pcc},k}} = \dfrac{\partial L_{\mathrm{T}}}{\partial \mathbf{x}_{\mathrm{pcc},k}} - \dfrac{\partial \mathbf{h}_{\mathrm{T},pcc,k}}{\partial \mathbf{x}_{\mathrm{pcc}k}} \mathbf{y}_{\mathrm{T},pcc,k} + \dfrac{\partial f_{\mathrm{T},pcc,k}}{\partial \mathbf{x}_{\mathrm{pcc}k}} = 0 k = 1, \cdots, N_{\mathrm{Dis}} \\ \dfrac{\partial L_{G-T}}{\partial \mathbf{w}_{\mathrm{pcc}k}} = -\mathbf{g}_{\mathrm{pcc}k} + \dfrac{\partial f_{\mathrm{T},pcc,k}}{\partial \mathbf{w}_{\mathrm{pcc}k}} = 0 k = 1, \cdots, N_{\mathrm{Dis}} \\ \dfrac{\partial L_{G-T}}{\partial \mathbf{y}_{\mathrm{T},pcc,k}} = -\mathbf{h}_{\mathrm{T},pcc,k} + \widetilde{\mathbf{S}}_{\mathrm{pcc}k} + \dfrac{\partial f_{\mathrm{T},pcc,k}}{\partial \mathbf{y}_{\mathrm{T},pcc,k}} = 0 k = 1, \cdots, N_{\mathrm{Dis}} \end{cases} \tag{B-9}$$

$$\frac{\partial L_{G-D_k}}{\partial(\Phi_{\mathrm{D}_k},\Phi_{\mathrm{pcc}k})}=0 \;\Leftrightarrow\; \begin{cases} \frac{\partial L_{G-D_k}}{\partial \mathbf{x}_{\mathrm{D}_k}}=\frac{\partial L_{\mathrm{D}_k}}{\partial \mathbf{x}_{\mathrm{D}_k}}+\frac{\partial \mathbf{h}_{D_k,pcc}}{\partial \mathbf{x}_{\mathrm{D}_k}}\mathbf{y}_{D_k,pcc}+\frac{\partial f_{D_k,pcc}}{\partial \mathbf{x}_{\mathrm{D}_k}}=0 \\ \frac{\partial L_{G-D_k}}{\partial \mathbf{u}_{\mathrm{D}_k}}=\frac{\partial L_{\mathrm{D}_k}}{\partial \mathbf{u}_{\mathrm{D}_k}}+\frac{\partial f_{D_k,pcc}}{\partial \mathbf{u}_{\mathrm{D}_k}}=0 \\ \frac{\partial L_{G-D_k}}{\partial \mathbf{S}_{\mathrm{pcc}k}}=\frac{\partial f_{D_k,pcc}}{\partial \mathbf{S}_{\mathrm{pcc}k}}-\mathbf{y}_{D_k,pcc}=0 \\ \frac{\partial L_{\mathrm{G}-D_k}}{\partial \mathbf{y}_{\mathrm{D}_k}}=-\mathbf{h}_{\mathrm{D}_k}+\frac{\partial f_{D_k,pcc}}{\partial \mathbf{y}_{\mathrm{D}_k}}=0 \\ \frac{\partial L_{G-D_k}}{\partial \mathbf{w}_{\mathrm{D}_k}}=-\mathbf{g}_{\mathrm{D}_k}+\frac{\partial f_{D_k,pcc}}{\partial \mathbf{w}_{\mathrm{D}_k}}=0 \\ \frac{\partial L_{G-D_k}}{\partial \mathbf{y}_{D_k,pcc}}=-\mathbf{S}_{\mathrm{pcc}k}+\mathbf{h}_{D_k,pcc}+\frac{\partial f_{D_k,pcc}}{\partial \mathbf{y}_{D_k,pcc}}=0 \end{cases} \tag{B-10}$$

Therefore, the auxiliary functions $f_{T,pcc,k}$ and $f_{\mathrm{D}_k,\mathrm{pcc}}$ ($k=1,\cdots,N_{\mathrm{Dis}}$) in the distributed model must meet the following requirements.

$$\begin{cases} \frac{\partial f_{\mathrm{T,pcc},k}}{\partial \mathbf{x}_{\mathrm{T}}}=0 \quad \frac{\partial f_{\mathrm{T,pcc},k}}{\partial \mathbf{u}_{\mathrm{T}}}=0 \\ \frac{\partial f_{\mathrm{T},pcc,k}}{\partial \mathbf{w}_{\mathrm{T}}}=0 \quad \frac{\partial f_{\mathrm{T},pcc,k}}{\partial \mathbf{y}_{\mathrm{T}}}=0 \quad \frac{\partial f_{\mathrm{T},pcc,k}}{\partial \mathbf{w}_{\mathrm{pcc}k}}=0 \quad \frac{\partial f_{\mathrm{T},pcc,k}}{\partial \mathbf{y}_{\mathrm{T},pcc,k}}=0 \\ \frac{\partial f_{\mathrm{T,pcc},k}}{\partial \mathbf{x}_{\mathrm{pcc},k}}=\frac{\partial L_{\mathrm{D}_k}}{\partial \mathbf{x}_{\mathrm{pcc},k}}+\frac{\partial \mathbf{h}_{\mathrm{D}_k,\mathrm{pcc}}}{\partial \mathbf{x}_{\mathrm{pcc},k}}\mathbf{y}_{\mathrm{D}_k,\mathrm{pcc}} \\ \frac{\partial f_{\mathrm{D}_k,\mathrm{pcc}}}{\partial \mathbf{S}_{\mathrm{pcc},k}}=\mathbf{y}_{\mathrm{T,pcc},k} \\ \frac{\partial f_{D_k,pcc}}{\partial \mathbf{y}_{\mathrm{D}_k}}=0 \quad \frac{\partial f_{D_k,pcc}}{\partial \mathbf{w}_{\mathrm{D}_k}}=0 \quad \frac{\partial f_{D_k,pcc}}{\partial \mathbf{y}_{D_k,pcc}}=0 \\ \frac{\partial f_{\mathrm{D}_k,\mathrm{pcc}}}{\partial \mathbf{x}_{\mathrm{D}_k}}=0 \quad \frac{\partial f_{\mathrm{D}_k,\mathrm{pcc}}}{\partial \mathbf{u}_{\mathrm{D}_k}}=0 \end{cases} \tag{B-11}$$

To effectively exploit the master-slave characteristics of the TN and DNs, some boundary sensitivities (α_k, β_k) are introduced to represent the auxiliary functions, as well as to reflect the influence of local boundary variations on neighbor networks. The auxiliary functions $f_{T,pcc,k}$ and $f_{\mathrm{D}_k,\mathrm{pcc}}$ can be expressed as (B-12), (B-13) based on the linear approximation.

$$f_{\mathrm{T,pcc},k}=\alpha_k^{\mathrm{T}}\mathbf{x}_{\mathrm{pcc},k} \quad k=1,\cdots,N_{\mathrm{Dis}} \tag{B-12}$$

$$f_{\mathrm{D}_k,\mathrm{pcc}}=\beta_k^{\mathrm{T}}\mathbf{S}_{\mathrm{pcc},k} \quad k=1,\cdots,N_{\mathrm{Dis}} \tag{B-13}$$

$$\alpha_k=\frac{\partial L_{\mathrm{D}_k}}{\partial \mathbf{x}_{\mathrm{pcc},k}}+\frac{\partial \mathbf{h}_{\mathrm{D}_k,pcc}}{\partial \mathbf{x}_{\mathrm{pcc},k}}\mathbf{y}_{\mathrm{D}_k,pcc}=\frac{\partial f_{\mathrm{D}_k}}{\partial \mathbf{x}_{\mathrm{pcc},k}}-\frac{\partial \mathbf{h}_{\mathrm{D}_k}}{\partial \mathbf{x}_{\mathrm{pcc},k}}\mathbf{y}_{\mathrm{D}_k}-\frac{\partial \mathbf{g}_{\mathrm{D}_k}}{\partial \mathbf{x}_{\mathrm{pcc},k}}\omega_{\mathrm{D}_k}+\frac{\partial \mathbf{h}_{\mathrm{D}_k,pcc}}{\partial \mathbf{x}_{\mathrm{pcc},k}}\mathbf{y}_{\mathrm{D}_k,pcc} \quad k=1,\cdots,N_{\mathrm{Dis}} \tag{B-14}$$

where $\beta_k=\mathbf{y}_{\mathrm{T},pcc,k}$, is a boundary sensitivity vector obtained from TN control center which means the influences of the k^{th} DN on the TN by boundary real and reactive power; α_k is a boundary sensitivity vector obtained from the k^{th} DN control center, represents the influence of the TN on the k^{th} DN by boundary state variable vector ($\mathbf{x}_{\mathrm{pcc}k}$).

Appendix C. Supplementary data

Supplementary data associated with this article can be found, in the online version, at https://doi.org/10.1016/j.ijepes.2018.07.019.

References

[1] Martins VF, Borges CLT. Active distribution network integrated planning incorporating distributed generation and load response uncertainties. IEEE Trans Power Syst 2011;26:2164–72.
[2] Tonkoski R, Turcotte D, El-Fouly THM. Impact of high PV penetration on voltage profiles in residential neighborhoods. IEEE Trans Sustain Energy 2012;3:518–27.
[3] Kulmala A, Repo S, Järventausta P. Coordinated voltage control in distribution networks including several distributed energy resources. IEEE Trans Smart Grid 2014;5:2010–20.
[4] Li P, Ji H, Wang C, et al. Coordinated control method of voltage and reactive power for active distribution networks based on soft open point. IEEE Trans Sustain Energy 2017;8:1430–42.
[5] Kim BH, Baldick R. Coarse-grained distributed optimal power flow. IEEE Trans Power Syst 1997;12:932–9.
[6] Kim BH, Baldick R. A comparison of distributed optimal power flow algorithms. IEEE Trans Power Syst 2000;15:599–604.
[7] Conejo AJ, Aguado JA. Multi-area coordinated decentralized DC optimal power flow. IEEE Trans Power Syst 1998;13:1272–8.
[8] Tomaso E. Distributed optimal power flow using ADMM. IEEE Trans Power Syst 2015;3:1005–11.
[9] Sulc P, Backhaus S, Chertkov M. Optimal distributed control of reactive power via the alternating direction method of multipliers. IEEE Trans Energy Conversion 2014;29:968–77.
[10] Yan W, Wen L, Li W. Decomposition–coordination interior point method and its application to multi-area optimal reactive power flow. Electrical Power Energy Syst 2011;33:55–60.
[11] Mauricio GE, Marcos JR, Mantovani JRS, et al. Decentralized AC power flow for real-time multi-TSO power system operation. In: Proc. IEEE PES General meeting, 2010. pp. 1–7.
[12] Lin C, Wu W, Zhang B, et al. Decentralized reactive power optimization method for transmission and distribution accommodating large-scale DG integration. IEEE Trans Sustain Energy 2017;1:363–73.
[13] Marinescu B, Bourles H. Robust predictive control for the flexible coordinated secondary voltage control of large-scale power systems. IEEE Trans Power Syst 1999;14:1262–8.
[14] Wang HF, Li H, Chen H. Coordinated secondary voltage control to eliminate voltage violations in power system contingencies. IEEE Trans Power Syst 2003;18:588–95.
[15] Sun H, Guo Q, Zhang B, et al. Master–slave splitting based distributed global power flow method for integrated transmission and distribution analysis. IEEE Trans Smart Grid 2015;6:1484–92.
[16] Huang Q, Vittal V. Integrated transmission and distribution system power flow and dynamic simulation using mixed three-sequence/three-phase modeling. IEEE Trans Power Syst 2017;32:3704–14.
[17] Sun H, Zhang B. Global state estimation for whole transmission and distribution networks. Electr Power Syst Res 2005;74:187–95.
[18] Zhao J, Fan X, Lin C. A distributed continuation power flow method for integrated transmission and active distribution grid, Journal of Modern Power Systems and Clean. Energy 2015;3:103–13.
[19] Li Z, Guo Q, Sun H. A new LMP-sensitivity-based heterogeneous decomposition for transmission and distribution coordinated economic dispatch. IEEE Trans Power Syst 2013;28:1140–8.
[20] Li Z, Wang J, Sun H, et al. Transmission contingency analysis based on integrated transmission and distribution power flow in smart grid. IEEE Trans Power Syst 2015;30:3356–67.

[21] Li Z, Guo Q, Sun H. Coordinated transmission and distribution AC optimal power flow. IEEE Trans Smart Grid 2018;9:1228–40.
[22] Gabash A, Li P. Active-reactive optimal power flow for low-voltage networks with photovoltaic distributed generation. In: 2nd IEEE International Energy Conference and Exhibition, 2012. pp. 381–386.
[23] Gabash A, Xie D, Li P. Analysis of influence factors on rejected active power from active distribution networks, IEEE Power and Energy Summit (PESS), 2012. pp. 25–29.
[24] Gabash A, Li P. On variable reverse power flow-part I: Active-Reactive optimal power flow with reactive power of wind stations. Energies 2016;9:121–32.
[25] Gabash A, Li P. On variable reverse power flow-part II: an electricity market model considering wind station size and location. Energies 2016;9:235–47.
[26] Konopinski RJ, Vijayan P, Ajjarapu V. Extended reactive capability of DFIG wind parks for enhanced system performance. IEEE Trans Power Syst 2009;24:1346–55.
[27] Zou K, Agalgaonkar AP, Muttaqi KM. Distribution system planning with incorporating DG reactive capability and system uncertainties. IEEE Trans Sustain Energy 2012;3:112–23.
[28] Liu WH, Papalexopoulos AD, Tinney WF. Discrete shunt controls in a newton optimal power flow. IEEE Trans PAS 1992;7:1509–18.
[29] Liu M, Tso SK, Cheng Y. An extended nonlinear primal-dual interior-point algorithm for reactive-power optimization of large-scale power systems with discrete control variables. IEEE Trans Power Syst 2002;17:982–91.
[30] Soler EM, Asada EN, Costa GRM. Penalty-based nonlinear solver for optimal reactive power dispatch with discrete controls. IEEE Trans Power Syst 2013;28:2174–82.